Study Protocol

Numerical analysis study on seismic performance of semi-rigid steel frame infilled with prefabricated composite wall panels

Abstract: The semi-rigid connected steel frame has good displacement ductility and energy dissipation capacity, and the interaction between the traditional steel frame and the filled wall is the critical factor affecting its seismic performance. In this paper, for the semi-rigid steel frame, the composite wall panel and the frame are separated by foam concrete mortar, and the effective connection isachieved by the tensioned steel bar. The premature brittle failure of composite wall panels can be preventedusing friction energy dissipation between wall panels.By using ABAQUS simulation method, a semi-rigid steel frame composite wall is established. The failure mode, hysteresis curve and skeleton curve of simulation and test are compared and analyzed, and the reliability of the model is proved.The finite element model with thedifferent number of wall panels is established to analyze its influence on the seismic performance of the structure.The results show that the frame structure realizes the effective connection between the composite wall panel and the concrete-filled steel tube frame, which jointly resists the earthquake action and reduces the damage of the earthquake action to the filled wall. With the increase in the number of composite wall panels, the ultimate load decreases gradually. The initial stiffness of the four layers of wall panels is more significant and decreases rapidly. When the wall panel has three or four layers, the energy dissipation capacity of the specimen is the strongest.The two are relatively close, stable at 24.48, and the increase is 5.15% compared with the second layer of the wall panel, and the increase is 12.72% compared with the third layer of the wall panel.

Key words: Semi-rigid steel frame; Foam concrete; Seismic performance; ABAQUS;

1Introduction

Semi-rigid connected steel frames have remarkable displacement ductility and energy consumption ability[1-3].However, the lateral stiffness and strength of the frame will decrease under the action of earthquake[4-6]. To improve the stiffness and strength of the structure, many scholars have proposed various acceptable methods for strengthening the system,such as enhancing the stiffness of connectors[7], improving the stiffness of supporting members[8], and enhancing the stiffness of steel plate filling walls[9].At the same time, on the one hand, the masonryfilled wall provides a sizeable lateral stiffness of the structure, reduces the interstory displacement of the structure, absorbs part of the seismic shear force, dissipates the seismic energy, and plays a favorable role in the seismic resistance of the structure. On the other hand, due to the excessive weight, stiffness and brittleness of the masonryfilled wall itself, the energy absorbed by the whole structure is also increased. The filled wall is more prone to failure. This energy is unfavorable to the seismic performance of the whole frame structure after failure [10-13].

At present, there are many researches on the earthquake resistance of filled wall and frame together[14-15]. Mohammadi [16] designed a friction-slip fuse placed in the center of the infill wall to limit or eliminate damage to the infill wall and frame.A. Karaduman [17], through a large number of experiments, shows that the filled wall can increase the resistance of the structure to earthquake, and can absorb more energy through the shear and friction of the wall frame nodes.

To overcome these problems, a new steel frame

system is proposed in this paper: a semi-rigid steel frame infilled with prefabricated composite wall panels; the composite wall panel is divided into multiple layers, and separated from the surrounding frame, there is a horizontal sliding joint between the wall panels, and with the aid of foam concrete mortar bonded into a whole. The frame system can not only give full play to the excellent ductility of the semi-rigid steel frame, but also improve the seismic performance of the composite wall through the sliding damping mechanism, and avoid the premature shear failure of the composite wall panel due to the harmful interaction between the frame and the composite wall.

In this paper, ABAQUS finite element analysis software is used to conduct separate numerical modeling of semi-rigid connected steel frame and composite wall panel. The applicability of the numerical model and the accuracy of parameter selection is verified by comparative test results, and the bearing capacity and deformation law of semi-rigid connected steel frame and wall layer number under horizontal earthquake are studied.

2Construction of FEM model

2.1 Introduction to test model

Fig. 1(a)(b) shows the schematic of the structure: semi-rigid steel frame infilled with prefabricated composite wall panels. The frame structure mainly consists of a semi-rigid steel frame, wall panels, damping layers (i.e., low-strength mortar sliding joints), tensioned steel bar and steel wire mesh.

Q235 H-section steel is used for the beams and columns. The cross-section of the beam and column is 194mm×150mm×6mm×9mm and 175mm×175 mm×7.5mm×11mm, respectively.

Fig. 1(c)(d) shows the detailed construction of strip composite wallboard.The composite wall is composed of strip composite wall panels spliced by tongue and groove joint. Strip type composite wall panel length 3540mm, thickness 240mm, height 590mm. In the thickness direction, the strip composite wall panel is divided into three layers.The middle is 80mm graphite polystyrene board insulation layer; the two sides are 80mm foamed concrete structural layer.

The cube compressive strength of the foam concrete wall panel is 3.8MPa. The vertical load with 499.5kN is applied to each concrete-filled steel tube column and kept constant. The horizontal load is applied through the beam axis direction, and the whole displacement is controlled. The test loading direction is positive when pushed out by jack and negative when pulled back. When the test specimen has a large deformation and loses its bearing capacity, the test load is stopped.

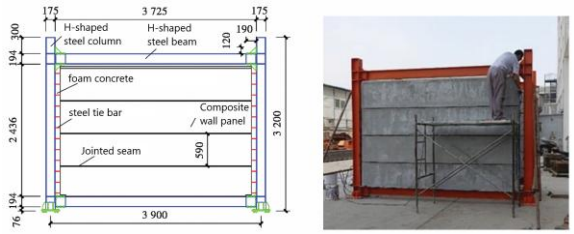

(a) Geometric dimension (b) Test picture

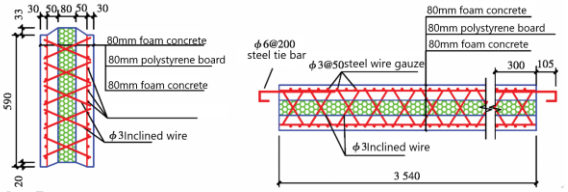

(c) Longitudinal section(d) Transverse section

Fig. 1.The detailed dimensions and reinforcement

Fig. 2 shows the pseudo-static loading schedule according to Chinese code Building Seismic Test Regulations (JGJ/T 101–2015) [18]. Note thatthe interstory drift (ISD) of the specimen is back-calculated by the loading protocol subjected to the top steel beam. Incremental inter-story displacement of the first four loading steps is 3.45 mm (represented to ISD of 0.125%), the incremental interlayer displacement of the middle five loading steps is 6.9 mm,and the after displacement increases to 13.8 mm.

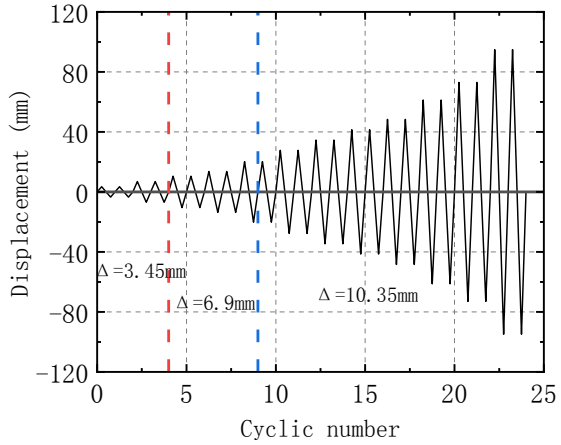

Fig. 2. Loading protocol.

2.2 Cell types and interactions

2.2.1 Main body frame

Solid element C3D8R (i.e., three-dimensional solid reduction integral element) is used for the concrete filled steel tube column, H-beam, connecting plate and bolt. Compared with the ordinary complete integral element, the 8-node reduction integral element uses one less integral point in each direction, reducing the calculation amount of the model and improving the accuracy of the model calculation. The deformation and stress of the foundation beam are not considered, so the rigid body element is used for simulation.

The friction coefficient is 0.4 between the concrete column and the steel pipe. The left and right ends of the upper H-shaped steel beam are anchored with 12 M12 high-strength bolts and the connecting plate, and the pre-tightening force of the bolts is set to 32kN.

2.2.2 Steel bar element

Due to the slender material characteristics of the steel bar, it can only withstand the tensile and compression action but not the transverse shear action, which is consistent with the truss element, so the rebar is simulated by T3D2 element (two-node linear three-dimensional truss element).

In the numerical analysis, the adhesive slip between the foamed concrete and the steel mesh is ignored, and it is Embedded into the wall panel, and connected to the main frame by the tie bar.

2.2.3 Foam concrete wall panels

The foamed concrete wall panel is regarded as a continuous homogeneous material, and the model is easy to converge under cyclic load using the quadratic reduction integral element C3D8R.

Table 1 shows the contact parameters between the four-layer foamed concrete composite wall panel and the wall panel and the frame. The sliding friction between the adhesion of mortar and the composite wall panel is simulated by cohesion + Coulomb friction criterion.

Table 1 Contact interface parameters

contact surface	rigidity (MPa/mm)			peak stress（MPa）			G_f^I	μ
	K_{nn}	K_{ss}	K_{tt}	t_n^0	t_s^0	t_t^0	(N/ mm)	
Wall to wall	82	36	36	0.55	0.5	0.5	0.04	0.2
Wall to frame	82	36	36	0.275	0.25	0.25	0.02	0.4

2.3 Constitutive model of materials

2.3.1 Constitutive relation of steel

The steel adopts the double broken line constitutive model. Before it reaches the yield point, the steel is regarded as a linear elastic material, where the break line slope is Young's model Es, and after the yield point is reached, the steel is regarded as a plastic material. Table 2 shows the parameters of the steel.

Table 2 Mechanical properties of steel

Type of steel	f_y/MPa	f_y/MPa	E/GPa
steel tie bar	405.0	581.0	206.9
steel fabric	662.0	718.0	190.8
square steel	373.0	444.3	218.2
steel beam	296.0	453.0	202.2
connecting	318.0	468.0	202.9

2.3.2 Constitutive relation of concrete

The stress-strain curve of concrete under uniaxial tension can be determined by:

$$\sigma = (1 - d_t)E_c\varepsilon$$

$$d_t = \begin{cases} 1 - \rho_t[1.2 - 0.2x^5] x \le 1 \\ 1 - \dfrac{\rho_t}{a_t(x-1)^{17} + x} x > 1 \end{cases}$$

$$\boldsymbol{x} = \frac{\boldsymbol{\varepsilon}}{\boldsymbol{\varepsilon}_{t,r}} \rho_t = \frac{f_{t,r}}{E_c \varepsilon_{t,r}}$$

Here a_t is the parameter value of the descending section of the uniaxial tensile stress-strain curve of concrete. $f_{t,r}$ represents the uniaxial tensile strength of concrete. $\boldsymbol{\varepsilon}_{t,r}$ is the peak tensile strain of concrete corresponding to the representative value of uniaxial tensile strength. d_t is the evolution coefficient of concrete uniaxial tensile damage.

The stress-strain curve of concrete under uniaxial compression can be determined by:

$$\sigma = (1 - d_c) E_c \varepsilon$$

$$d_c = \begin{cases} 1 - \dfrac{\rho_c n}{n - 1 + x^n} x \le 1 \\ 1 - \dfrac{\rho_c}{a_c(x-1)^2 + x} x > 1 \end{cases}$$

$$\eta = \frac{E_c \varepsilon_{c,r}}{E_c \varepsilon_{c,r} - f_{c,r}} \rho_c = \frac{f_{c,r}}{E_c \varepsilon_{c,r}}$$

Here a_c is the parameter value of the descending section of the stress-strain curve of concrete under uniaxial compression; $f_{c,r}$ represents the uniaxial compressive strength of concrete; $\varepsilon_{c,r}$ is the peak tensile strain of concrete corresponding to the representative value of uniaxial compressive strength; d_c is the evolution coefficient of concrete uniaxial compression damage.

2.3.3 Constitutive model of foam concrete

As a new type of building material, autoclaved aerated block is rarely studied on its constitutive relationship. In this paper, the constitutive model of light filling wall material is adopted, and the expression of compressive stress-strain relationship can be determined by:

$$y = \begin{cases} x & x \le 0.5 \\ 2x - 1.1x^2 - 1.7x^3 + 3.8x^4 - 2x^5 & 0.5 < x \le 1.0 \\ \dfrac{5.2 + 3.7x}{1 + 7.9x} & 1.0 < x \le 4.0 \end{cases}$$

Here $x = \varepsilon/\varepsilon_{pr}, y = \sigma/\sigma_0$; ε_{pr} is the compressive strain value corresponding to the peak stress, which is 3.8MPa measured by the test. σ_0 is the peak compressive stress.

The expression of uniaxial tensile stress-strain relationship of foamed concrete can be determined by:

$$y = \begin{cases} x & x \le 1.0 \\ \dfrac{x}{\alpha_t(x-1)^{1.7} + x} & x \ge 1.0 \end{cases}$$

Here $x = \varepsilon/\varepsilon_{pt}, y = f/f_{pr}$; ε_{pt} is the tensile strain value corresponding to the peak stress; f_{pr} is the peak tensile stress, $\alpha_t = 0.312 f_t^2$.

Fig. 3. shows the finite element model of the frame composite wall established according to the above steps.

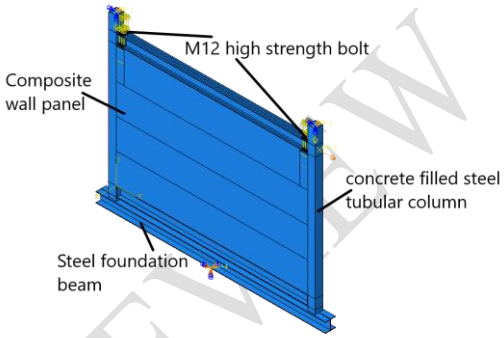

Fig. 3. Numerical model diagram

3Numerical results verification

Fig. 4. shows the stress comparison and concrete damage of the finite element model analysis results. The stress transmitted by the concrete-filled steel tube column is small and located at the four corners of the whole wall panel. The foamed concrete composite wall panels move each other in the process of lateral force, resulting in discontinuity of stress between the wall panels, so the composite wall panels are less damaged by compression. According to the damage of the composite wall panel, it can be seen that because there are only tension reinforcement bars at the joint of the composite wall panel and the frame column, the tensile damage of the edge of the concrete wall panel is more serious, and the crack trend is consistent with the test.

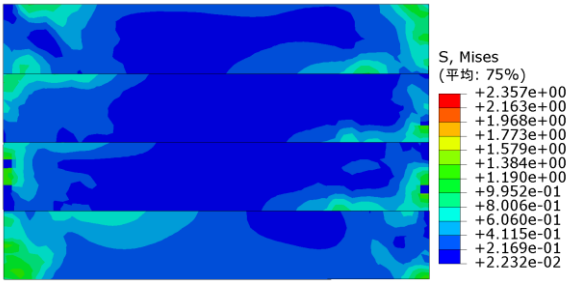

(a)

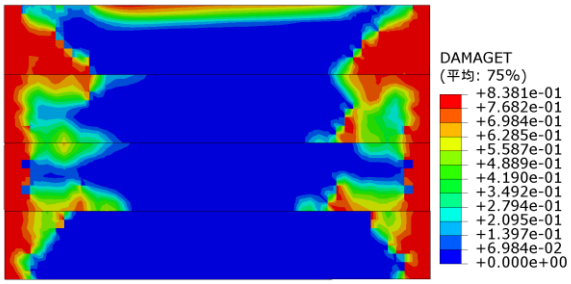

(b)

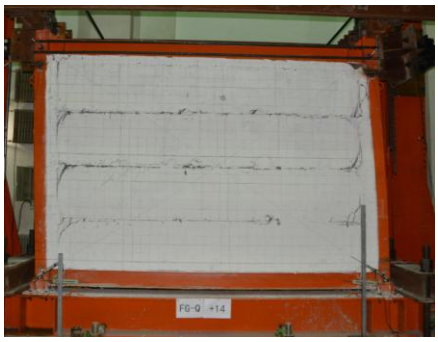

(c)

Fig.4.Stress nephogram(a), damage nephogram(b) and crack trend(c) of composite wall panel (unit: MPa).

Fig. 5. shows the simulation and test hysteresis curve and skeleton curve of the semi-rigid steel frame infilled with prefabricated composite wall panels. The hysteretic curve shows an inverse S-shape, and the pinch effect appears in the middle. Because the four layers of wall panels are bonded by foamed concrete, the composite wall panels first appear horizontal cracks at the joint, and then occur dislocation. When the horizontal load transferred to the composite wall panels exceeds the sum of the bonding force and friction of foamed concrete at the joint, the horizontal joint cracks. In the test, there are cracks in the tensile zone of concrete and the slip of steel bars, but the slip of concrete and steel bars is ignored in the finite element model, so the middle position of the simulated curve is relatively "full", and the slip phenomenon is more evident in the test. The skeleton curve in the early stage is different from the simulation because of the viscous action of mortar. However, with the loading of horizontal displacement, the viscous effect gradually disappeared. The interaction between wall panels gradually changed into frictional contact, and the skeleton curves of simulation and test results gradually agreed.

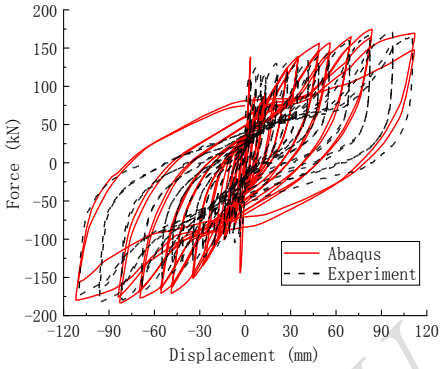

(a)

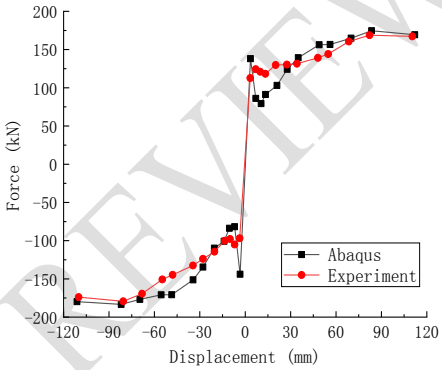

(b)

Fig.5.Contrast between hysteretic curve(a) and skeleton curve(b)

The whole loading process of the semi-rigid steel frame infilled with prefabricated composite wall panelsis simulated by the distributed modeling, and the reliability of the model is verified. The crack development, hysteretic curve and skeleton curve of the test model of semi-rigid steel frame composite wall are fitted. The stress nephogram, compression damage and displacement distance of foamed concrete composite wall panel are analyzed, and the results are satisfactory, which verifies the feasibility of the model established in this paper and the correctness of parameter selection.

4The influence of the number of wall panels

On the premise of determining the size of the semi-rigid steel frame infilled with prefabricated composite wall panels, the number of layers of composite wallboard is taken as the research object. Because the damage of the entire foamed concrete wall panel is relatively serious

during the loading process of the whole wall panel simulation calculation, only the influence of double, three, four and five layers on the seismic performance of the wall panels is analyzed.

4.1 Hysteretic curves

Fig. 6. shows the hysteresis curves of specimens SJ1 to SJ4. When the composite wallboard of the specimen is composed of two layers, the hysteresis curves show a "Z" shape, and the middle of the curve is relatively gentle, indicating that a large amount of slip occurs during loading.When the composite wall panels are three or four layers, the hysteresis curve is "S", and slip occurs during the loading process. At the initial stage of loading, due to the viscous action of mortar between each layer of wall panels, the load is large, then the viscous action disappears, and the viscous action between wall panels changes to Coulomb friction. When the composite wall board is five layers, the hysteresis curve is fusiform and not full, and compared with the previous several specimens, the mortar has a greater viscous effect and lasts longer before it turns into coulomb friction.

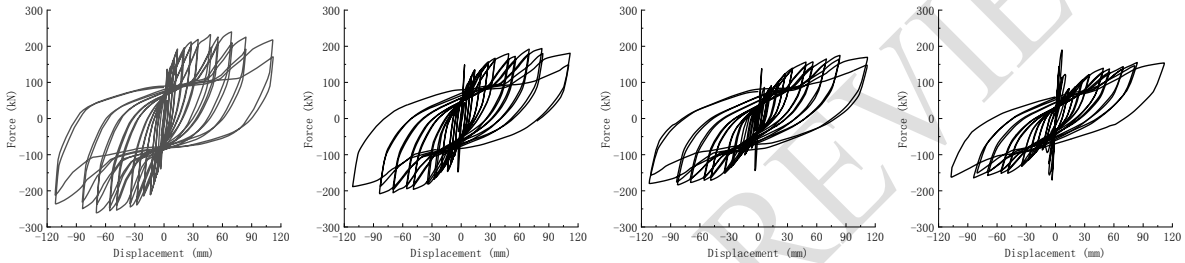

(a)(b) (c) (d)

Fig. 6. Hysteretic curves of specimens (a)SJ1, (b)SJ2,(c)SJ3,(d)SJ4

4.2 Skeleton curve

Fig. 7. shows the skeleton curves of the four specimens. SJ1 has a significantly stronger bearing capacity than other specimens, and enters the yield stage at the earliest. With the increase in the number of wall panels, the peak load decreases gradually.

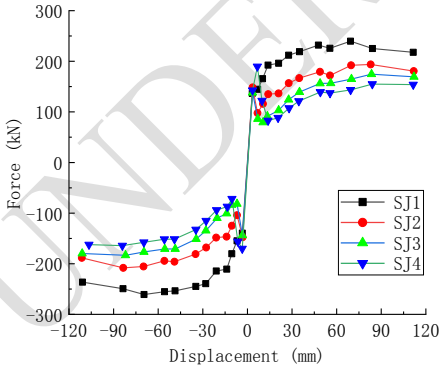

Fig. 7.Skeleton curve of specimens

4.3 Stiffness degradation

Secant stiffness can be used to describe the deformation, strength, and stiffness characteristics of specimens. The secant stiffness K_i of specimenscan be computed by:

$$K_j = \frac{|F_i^+| + |F_i^-|}{|X_i^+| + |X_i^-|}$$

Here,K_i is the secant stiffness of specimens at loading stage$i$;$F_i$is the maximum force at the i-th loading level and correspondingly X_i isthe peak displacement; + and – mean the positive and negative directions, respectively.

Fig. 8. shows the stiffness degradation curves of each specimen.At the initial stage of loading, due to the viscous action of mortar between the wall panels, the composite wall is bonded as a whole. The stiffness is stable at 42.94kN/mm, and the error is not more than 5%. With the increase of horizontal displacement, the viscosity of each specimen gradually disappeared. The viscosity of specimen SJ4 disappeared the latest due to the number of layers, and the stiffness gradually degraded from the maximum to the minimum. The final stiffness degradation of specimen SJ1 was the largest and stabilized at 2.042 kN/mm, while the rest stabilized at 1.556 kN/mm.

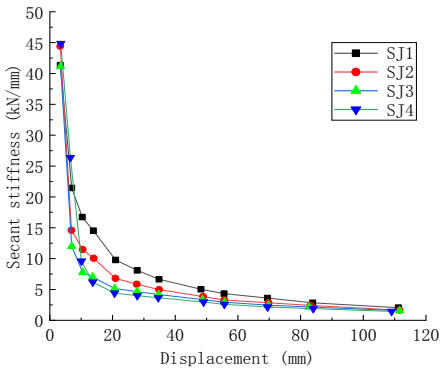

Fig. 8. Stiffness degradation curves of specimens.

4.4 Equivalent viscous damping ratio

As shown in the fig. 9, the energy dissipation capacity can be measured by equivalent viscous damping ratio h_e. The equivalent viscous damping ratio is characterized by:

$$h_e = \frac{1}{2\pi}\frac{S_{ABC} + S_{CDA}}{S_{OBE} + S_{ODF}}$$

where $S_{ABC} + S_{CDA}$ is the area surrounded by the hysteresis loop; $S_{OBE} + S_{ODF}$ is the area surrounded by the triangles OBE and ODF.

Fig.10. shows the equivalent viscous dampingcoefficients of the four groups of specimens. The energy dissipation stage can be divided into three stages: First, due to the viscous action of mortar between wall panels, the energy dissipation effect increases rapidly. With continuous loading, the concrete steel tube column gradually yields, and the energy dissipation capacity decreases as a whole. After that, due to the dislocation of the composite wall panels, friction energy consumption, the energy consumption capacity of the components increased rapidly. As the wall panel of specimen SJ1 is badly damaged, the friction energy consumption in the later period is reduced. SJ4 has the worst energy dissipation capacity because of the lowest ultimate bearing capacity, the most stratified wall panels and less relative slip. The energy dissipation capacity of SJ2 and SJ3 samples is the strongest, and they are close to each other, stable at 24.48, and increased by 5.15% compared with SJ1 and 12.72% compared with SJ4.

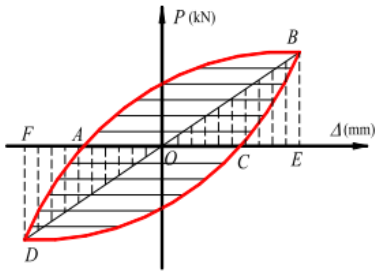

Fig. 9. Calculation of equivalent viscous damping coefficient.

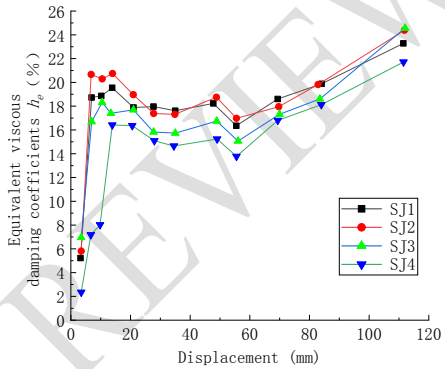

Fig. 10. Equivalent viscous damping coefficients.

5 Conclusions

（1）During the loading process, the composite wall panel and the semi-rigid connected steel frame are effectively connected through the tensioned steel reinforcement to jointly resist the earthquake action. Moreover, due to the misalignment of the wall panel, on the one hand, the stiffness of the semi-rigid steel frame infilled with prefabricated composite wall panels is reduced, and the stress between the wall panels is not coherent, which reduces the damage of the composite wall panel caused by the earthquake action. On the other hand, due to the friction of the four-layer composite wall plate under the reciprocating load, the energy dissipation capacity of the frame structure gradually increases after the yielding of the tensioned steel bars.

（2）By comparing and analyzing the hysteretic curve and skeleton curve of four different layers of composite wall panels, it is found that the ultimate load decreases gradually with the increase of the number of layers of composite wall panels, and when the wall panels are two

layers, the damage of composite wall panels is more serious, and the composite wall panels enter the descending stage at the earliest. When the wall plate has five layers, the bearing capacity is weaker than that of other specimens.

（3）Due to the viscous action of foamed concrete mortar between composite wall panels in the early stage of loading, the initial stiffness of the four groups of frame walls is relatively close, stable at 42.94kN/mm, and the error is not more than 5%. According to the equivalent viscous damping coefficient, the energy dissipation capacity of the frame structure is the strongest when the number of wallboard layers is three or four.

References

[1] J. Fang, W. Bao, F. Ren, et al, Behaviour of composite beams with beam-to-girder end-plate connection under hogging moments, Eng. Struct. (2021) 235.

[2] A.B. Sabbagh, s. Torabian, Semi-rigid floor-to-wall connections using side-framed lightweight steel structures: concept development, Thin-Walled Struct. (2021) 160

[3] M. Yekrangnia, P.G. Asteris, Multi-strut macro-model for masonry infilled frames with openings, J. Build. Eng. 32 (2020), 101683.

[4] W. Bao, J. Jiang, Y. Shao, et al., Experimental study of the lateral performance of a steel stud wall with a semi-rigid connected frame, Eng. Struct. 183 (2019) 677–689.

[5] A. Reyes-Salazar, M.D. Llanes-Tizoc, J. Bojorquez, et al., Force reduction factors for steel buildings with welded and post-tensioned connections, Bull. Earthq. Eng. 14 (2016) 2827–2858.

[6] Z. Li, J. Luo, M.J. He, et al., Seismic performance of multi-story glulam post-and-beam structures reinforced with knee-braces, J. Build. Eng. (2021) 44.

[7] B. Gil, R. Goni, E. Bayo, Major axis steel joint with additional plates subjected to torsion: stiffness characterization, Eng. Struct. 220 (2020).

[8] Y. Zhou, C. Gong, J. Zhao, G. Zhong, S. Tian, Strong-axis stability and seismic performance of perforated core plate buckling-restrained braces, Thin-Walled Struct. 156 (2020).

[9] W. Wang, Y. Ren, Z. Lu, J. Song, B. Han, Y. Zhou, Experimental study of the hysteretic behaviour of corrugated steel plate shear walls and steel plate reinforced concrete composite shear walls, J. Constr. Steel Res. 160 (2019) 136–152.

[10] M.J. Gombeda, C.J. Naito, S.E. Quiel, Development and performance of a ductile shear tie for precast concrete insulated wall panels, J. Build. Eng. 28 (2020).

[11] C. Zhang, W.Y. Huang, Y. Zhou, W.L. Luo, Experimental and numerical investigation on seismic performance of retrofitted RC frame with sector lead viscoelastic damper, J. Build. Eng. 44 (2021) 103218.

[12] Y. Ru, L. He, H. Jiang, Study on a new type of beam-column joint equipped with inclined tapered steel plates, J. Build. Eng. 45 (2022) 103581.

[13] A. Gu, Y. Zhou, R.S. Henry, et al., Simulation of shake-table test for a two-story low-damage concrete wall building, Struct. Control Health Monit. (2022), e3038.

[14] Brodsky A , Rabinovitch O , Yankelevsky D Z . Determination of the interaction between a masonry wall and a confining frame[J].Engineering Structures, 2018, 167:214-226.DOI:10.1016/j.engstruct.2018.04.001.

[15] Jingfeng Wang, Li Beibei. Cyclic testing of square CFST frames with ALC panel or block walls [J]. Journal of Constructional Steel Research, 2017, 130: 264-279.

[16] Tasnimi A A ,Mohebkhah A .Investigation on the behavior of brick-infilled steel frames with openings, experimental and analytical approaches[J].Engineering Structures, 2011, 33(3):968-980.

[17] Karaduman, A.; Polat, Z.; Kaltakci, M.Y. Statical analysis of infilled frames[J]. Structural Studies, Repairs, and Maintenance of Historical Buildings. 2001,7: - 425-433.

[18] Standard of China, JGJ/T 101-2015, Specification

for Seismic Test of Buildings, China Architectural and Building Press Beijing, 2015.